J Electroceram (2011) 27:66–77
DOI 10.1007/s10832-011-9651-x

Resistance variation in donor-doped PZT stacks with Cu inner electrodes under high field stress

Elmar Völkl · Philipp Hillebrand · Juergen Fleig

Received: 30 March 2011 / Accepted: 10 August 2011 / Published online: 24 August 2011

Abstract Changes of the resistance of donor-doped lead zirconate titanate (PZT) under high voltages were investigated at temperatures from 350 to 500°C in different gas atmospheres. Measurements on individual ceramic layers (about 75 μm thickness) of PZT multilayer stacks with Cu inner electrodes allowed numerous experiments on nominally identical PZT material. Under high fields, the conductivity decreased significantly on time scales much longer than needed for capacitor charging. At 350°C, for example, decay times of several 1000 s were found. The time constant of this conductivity decay depends exponentially on temperature with activation energies of about 1.3 eV in air. After interrupting the field stress, thermally activated (ca. 1.1 eV) relaxation of the conductivity was found on an even longer time scale. The results are interpreted in terms of oxygen vacancy motion under high fields (stoichiometry polarization) and diffusive relaxation. The importance of oxygen migration despite donor doping is attributed to the high PbO volatility of PZT which readily leads to significant oxygen deficiency. Oxygen diffusion coefficients are estimated.

Keywords PZT · Actuators · Electrical conductivity · Defects · Diffusion

1 Introduction

Perovskite-type oxides with large band gaps are widely used as electroceramics and play functional roles in numerous devices such as capacitors, piezoelectric actuators and transducers, filters, temperature and gas sensors, infrared cameras, etc. Three of the most prominent representatives of the wide range of compositions used in such applications are $SrTiO_3$, $BaTiO_3$ and $Pb(Zr_xTi_{1-x})O_3$ (PZT). Mass and charge transport properties of these materials are of high importance, either because of the functionalization of conduction (e.g. in sensors) or because current flow has to be avoided (e.g. in capacitors and piezoelectric applications). Thus, in-depth investigation of ion and electron motion and profound knowledge of the thermodynamics of defect concentrations is highly relevant. In case of $SrTiO_3$ and $BaTiO_3$, numerous research groups have worked on this topic for many years and a very high level of understanding of bulk defect chemistry and partly also of interfacial defect chemistry has already been achieved (see e.g. Refs. [1–26]). Such a detailed understanding is not available for many other perovskite-type electroceramics. For example, it is still far from being quantified under which doping, pressure and temperature conditions ionic or electronic conduction prevails in PZT and related materials [27–45], and also to what extent grain boundaries are either highly resistive or represent highly conductive paths for charge transport. Only recently, it was shown that in donor-doped PZT very pronounced oxygen tracer diffusion along grain boundaries may take place [46, 47].

The large difference in the knowledge of defect thermodynamics and kinetics of $SrTiO_3$/$BaTiO_3$ and PZT is also reflected in the discussion of conductivity variations taking place upon high field stress. For acceptor-doped $SrTiO_3$ and $BaTiO_3$, it was shown that drastic conductivity variations on a longer time scale can often be attributed to the motion of oxygen vacancies and their accumulation at the cathode or depletion at the anode [48–51]. Conductivity variations are thus essentially caused by Wagner-Hebb-type

E. Völkl · P. Hillebrand · J. Fleig (✉)
Christian Doppler Laboratory for Advanced Ferroic Oxides,
Institute of Chemical Technologies and Analytics,
Vienna University of Technology,
Getreidemarkt 9-164/EC,
1060 Vienna, Austria
e-mail: j.fleig@tuwien.ac.at

polarization with two ionically blocking electrodes [52–54]. Owing to space charge layers, grain boundaries act as barriers for oxygen vacancy motion and retard the resistance degradation process. The validity of this model was confirmed by local conductivity measurements on $SrTiO_3$ single and polycrystals [55, 56]. Donor dopants strongly stabilize the high-field resistance of $SrTiO_3$ and $BaTiO_3$ [48, 49, 57] and in case of La-doped $SrTiO_3$, for example, even after several hundred hours of high field stress at 350°C hardly any resistance change was found [48, 49]. This was attributed to the negligible concentration of oxygen vacancies in donor-doped materials.

A resistance decrease in bulk or thick film Pb-containing perovskites under high field stress is also reported, but mostly refers to experiments under high humidity conditions below 100°C [58–67]. There, migration of silver (or other) cations originating from the electrodes is often discussed as the major source of the degradation. Even though the position of paths enabling cation motion and also the exact mechanisms leading to conducting paths are still under debate, silver dendrite formation in grain boundaries, along micro-cracks or in pores are generally thought to be highly relevant. Silver migration in such specimens may thus be very similar to that discussed in many studies on the failure of microcircuits, where a voltage between silver electrodes on insulating substrates caused drastic resistance changes under humid conditions. Those changes were mostly explained by aqueous surface layers, allowing anodic dissolution and cathodic deposition of Ag^+ and thus enabling Ag dendrite growth [68–75].

At temperatures well above 100°C, conventional "aqueous" electrochemical motion of Ag ions, for example along hydrated surfaces or micro-cracks, becomes rather unlikely. Then the issue of high field conductivity variations in PZT has to be re-considered and phenomena similar to stoichiometry polarization in $SrTiO_3$ (see above) would hardly be surprising. Little data is available on conductivity variations in bulk samples of lead based perovskites under field at or above 200°C [33]. More information can be found on ferroelectric thin films (see e.g. Refs. [76–78]), but also there the situation is far from being understood: A number of different models was used to explain the very complex conduction phenomena occurring in these thin films and electrode/film interfaces seem to be highly important there.

In this contribution, we present a study on the resistance changes found in samples from donor-doped PZT multilayer stacks upon high fields. Temperatures were far above 100°C, i.e. conventional (aqueous) electrochemical electrode migration cannot be expected to play a role. Temperature and field were systematically varied, and the effect of the gas atmosphere was analyzed. Time constants of resistance changes and extent of the resistance variations were studied as well as the relaxation behavior after switching-off the fields. The results are discussed in the framework of field-induced stoichiometry changes.

2 Experimental

In order to easily achieve high fields in PZT and to be able to perform numerous different degradation experiments on identical but yet virgin PZT material, all measurements were performed on pieces of commercial 1.5% Nd doped PZT multilayer actuator stacks with a composition close to the morphotropic phase boundary (TDK-EPC, Deutschlandsberg, Austria). The stacks consist of numerous ceramic layers of about 75 µm thickness, separated by Cu inner electrodes, and were sintered in reducing atmosphere. Multilayer stacks were cut into pieces of ca. $8\times8\times1.5$ mm^3 such that the interdigital inner electrodes are located perpendicular to the large sample surface (Fig. 1(a)). All electrodes originating from one side of the sample were connected by an additional electrode stripe and were thus at an equipotential. The electrodes ending on the other side were isolated from each other (Fig. 1(b)). By contacting two neighboring inner electrodes by tungsten contact tips, a very local degradation experiment

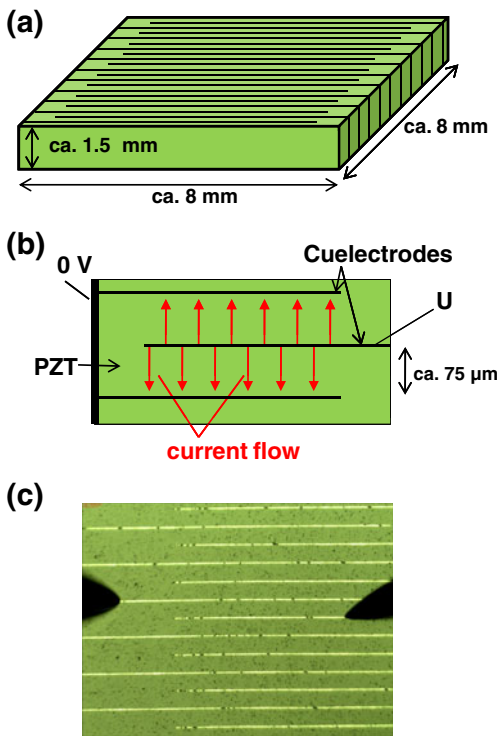

Fig. 1 Illustration of the sample and measurement geometry: (**a**) Sketch of a sample with interdigital Cu inner electrodes perpendicular to the large surface. (**b**) Sketch of a magnified top view of a sample, displaying three inner electrodes, two of them being connected on the left hand side (0 V). This leads to the current flow indicated by red arrows. (**c**) Photograph showing a sample part under the microscope with tips contacting two neighboring inner electrodes

could thus be performed, with the current flowing through two layers as indicated in Fig. 1(b). Figure 1(c) displays an optical image of the sample surface with the interdigital electrodes and the contact tips for electrical measurements. Moving the contact tips to other pairs on the same sample enabled interrogation of many layers and thus a systematic high field study on nominally identical PZT layers.

The stack pieces were placed on a ceramic heating table (Linkam, UK) and heated to 350–500°C set temperature. According to similar microelectrode measurements on well-known oxides such as YSZ single crystals [79–81], the true sample temperature in such experiments is not far from the set temperature. Conductivity measurements on entire stacks in a standard furnace as well as local measurements with an additional thermocouple on a reference sample indicate that the temperature difference between set and true sample temperature is of the order of 15–30°C. The flexibility given by the possibility of subsequently contacting numerous individual electrodes of a single stack piece by far counter-balances the disadvantage of the minor temperature uncertainty unavoidable in this set-up. In the following, we always refer to set temperatures and have to keep in mind that slightly lower sample temperatures are in reality expected.

All measurements were performed in the following manner: By means of a Keithley source measurement unit (2611), voltages between 20 and 200 V were applied to neighboring inner electrodes and thus fields between 0.27 MV/m and 2.7 MV/m were imposed. The current (measured by the same instrument) was detected at a rate of one measurement per second to one per minute (depending on temperature and rate of the resistance change). After times in the order of a few 10 s to several 1000 s (again depending on temperature), the current reached a more or less constant value and the high field was switched off. Relaxation of the modified resistance was then observed by a small probing voltage of 1 V and again measuring the current. Before and partly also after high field stress, impedance spectra were recorded by an Alpha station (Novocontrol, Germany) with an amplitude of 0.3 V in a frequency range of 1 MHz to 100 or 10 mHz. Most high field experiments were performed in ambient atmosphere. For comparison, a limited number of measurements were repeated in a reducing gas mixture of 2.5% H_2 in Ar.

Color changes between electrode pairs were observed in-situ (during high field stress) under a Mitutoyo microscope and characterized in more detail on quenched samples after the degradation or relaxation experiments by using a Zeiss AxioImager M1m microscope. The results presented in the following are based on much more than a hundred degradation experiments on several PZT stack pieces. This large number of measurements indicates that similar studies on larger PZT samples with only two electrodes would have been extremely time-consuming, compared to this study on samples with numerous inner electrodes.

3 Results

Impedance spectra, measured between 225 and 550°C without any high field stress, show a single arc in the complex impedance plane (see Fig. 2). Accordingly, the sample can be described by a single resistive and a (non-ideal) capacitive element. Hence, we suggest that the entire resistance of the PZT layers is determined either by the bulk conductivity of the PZT grains or by highly conducting grain boundaries. The latter contribute to the same arc as the bulk resistance [82–84]. However, also a third scenario cannot be completely excluded: very extended resistive space charge zones at grain boundaries may cover the entire grains and then again only a single arc results in the complex impedance plane with the resistance being that of the grain boundary space charge while the capacitance still that of the bulk [85]. Such a situation was recently observed in nano-crystalline $SrTiO_3$ [85, 86]. From the impedance measurements, averaged conductivities of PZT can be calculated and the corresponding Arrhenius plot is given in Fig. 3. An activation energy of approx. 1.4 eV is found, even though below the Curie temperature (around 350°C), a slightly higher activation energy might also be concluded.

In the following analysis, it is important that the angular relaxation frequencies (ω_r) of the impedance measurements are between several kHz at 500°C and ca. 0.2 Hz at 350°C. The relaxation frequency denotes the frequency for which the absolute value of the imaginary part of the impedance is at its maximum. In dc experiments, charging of the sample capacitor can be expected on the time scale of $1/\omega_r$ and thus within a few 10 s at 350°C and a few milliseconds at 500°C, respectively. Changes for times $>>1/\omega_r$ cannot be attributed to conventional capacitor charging. In our experi-

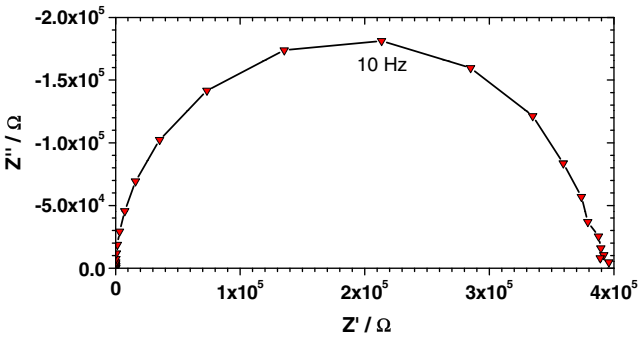

Fig. 2 Impedance spectrum measured at 400°C. The label in the plot indicates the frequency f of the data point which is closest to the angular relaxation frequency $\omega_r = 2\,\pi f_r$

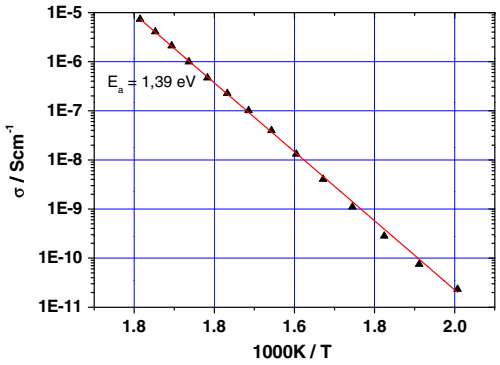

Fig. 3 Temperature dependence of the conductivity of the PZT layers

ments under high fields, the conductivity continuously decreased on a much longer time scale (many 1000 s at 350°C and several seconds at 500°C) and reached a virtually constant value after a certain time. Representative curves are shown for 350°C and 450°C in Fig. 4 (a,b). Conductivity changes up to about a factor of 4–5 were observed. It should be mentioned that the plateau being reached after some time was only an apparent one, since particularly at or above ca. 400°C the conductivity again increased on an even longer time scale (Fig. 4(c)) and often ended in a current break through. These additional long-term changes, however, are believed to reflect an independent degradation feature and are not further discussed in this publication.

After having reached the (apparent) plateau, the high voltage was disconnected and the conductivity started to increase again, at least for temperatures at or above 400°C (Fig. 5). This relaxation (probed by a 1 V dc signal) was much slower than the conductivity decrease. Only little relaxation was found for 350°C within the time scale used in this study (<1 day, Fig. 6(a)). In case of a sufficiently fast relaxation, the final conductivity was again rather close to the starting value before application of the large field. This seems to contradict the conductivity versus time curve shown in (Fig. 6(b)), since there the final value is smaller than the extrapolated starting conductivity. However, this apparent discrepancy is partly caused by the fact that the measured conductivity exhibits some non-linearity: Fig. 6(c) shows the non-linearity measured for different temperatures, with the conductivity in all cases being simply calculated from the current (shortly after applying the voltage) divided by the voltage. Hence, the lower conductivity after relaxation in Fig. 6(b) partly reflects the different probing voltage, which was 180 V during conductivity decrease and 1 V for the relaxation phase. Moreover, even voltages of 1 V can lead to a slight conductivity decrease after long times, and this may further contribute to some differences between starting and end values.

The changes in PZT due to high field stress also lead to some distortion of the corresponding impedance spectra: Fig. 7(a) shows spectra measured after a conductivity decrease under 200 V at 450°C. The distortion is an

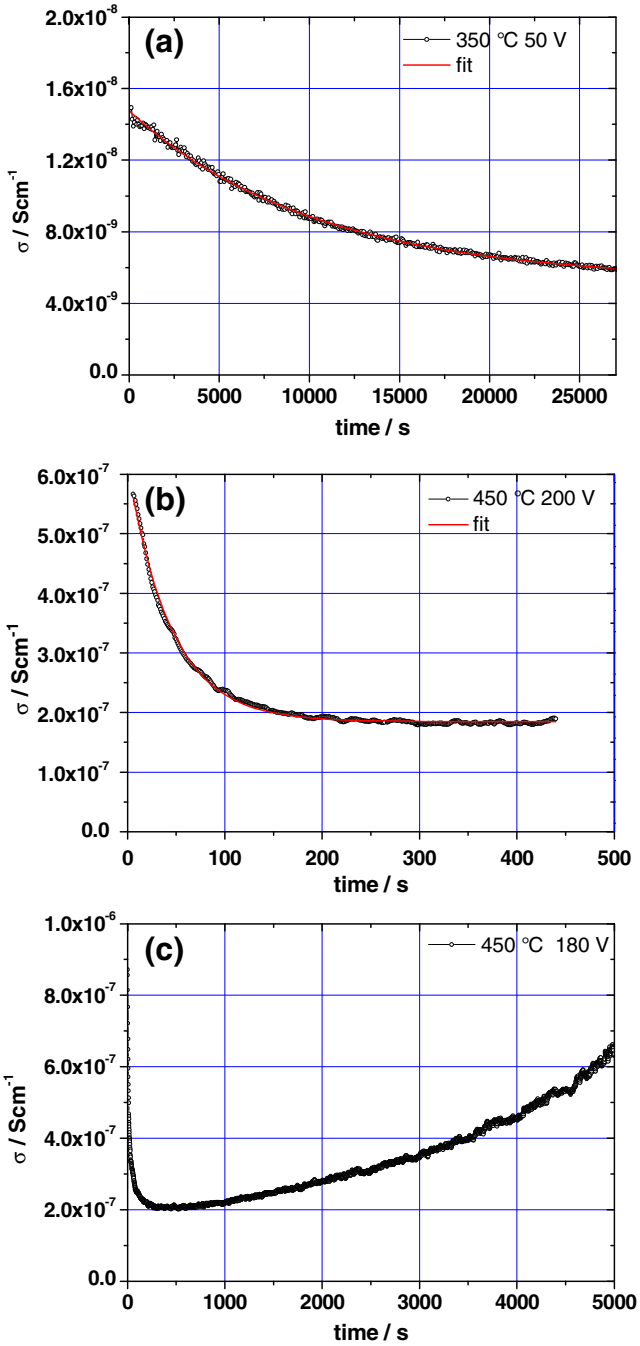

Fig. 4 Conductivity decrease during application of a high field: (**a**) for 350°C and 50 V; (**b**) for 450°C and 200 V; the fit lines are calculated according to Eq. 1. (**c**) Conductivity variations during high field stress of 180 V at 450°C on a longer time scale, indicating a conductivity decrease as in (**a**) and (**b**), but also a much slower conductivity increase

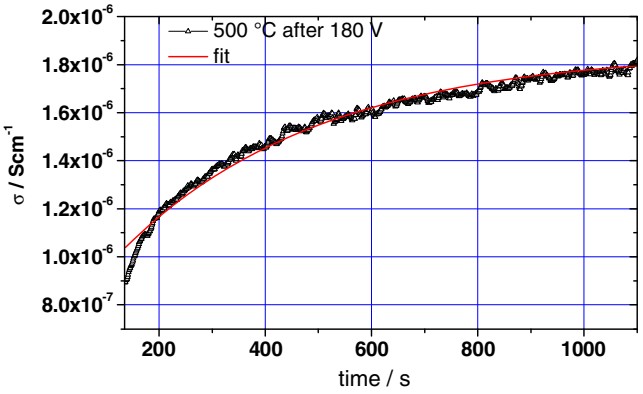

Fig. 5 Relaxation of the conductivity after disconnecting the voltage of 180 Vat 500°C. The high voltage was applied for 135 s. The fit line is calculated according to Eq. 2

indication that conductivity inhomogeneities in the layer might have built up. The decreasing size of the arc reflects the relaxation towards the original state. An exact localization of the sample region with enhanced resistivity after high field load was not possible yet and would require microelectrode measurements similar to those in Refs. [55, 56, 87, 88]. Hence, it remains an open question, whether the conductivity mainly decreases in the region close to the cathode or primarily close to the anode or even in the entire PZT layer.

For further quantification of the conductivity decrease, fits to the conductivity (σ) versus time (t) were made according to

$$\sigma = \sigma_{t=\infty} + (\sigma_{t=0} - \sigma_{t=\infty}) \cdot e^{-t/\tau_1} \quad (1)$$

with the fitting parameters $\sigma_{t=\infty}$, $\sigma_{t=0}$ and τ_1 denoting the high field conductivity after conductivity decrease (plateau value), the high field conductivity before the decrease, and the decay time, respectively. Examples of fitting curves are given in Fig. 4 and show that Eq. 1 describes the time dependence rather well. Similarly, the conductivity relaxation was quantified by

$$\sigma = \sigma'_{t=\infty} + (\sigma'_{t=t_0} - \sigma'_{t=\infty}) \cdot e^{-t/\tau_2}. \quad (2)$$

In Eq. 2, the fitting parameters were the low field conductivity when starting the relaxation $\sigma'_{t=t_0}$, the final conductivity after relaxation $\sigma'_{t=\infty}$, and the relaxation time τ_2. A typical fitting curve is shown in Fig. 5. It nicely fits the major part of the curve, but is non-ideal in the very first part of the relaxation.

The extent of the conductivity decrease can be described by $\sigma_{t=0} / \sigma_{t=\infty}$, which is identical to the factor of resistance increase of the PZT layer during high field stress. It is shown in Fig. 8 that this resistance increase (conductivity decrease) depends on voltage. In particular for higher temperatures (at or above 400°C), the extent to which the resistance increases clearly increases with the voltage. This is indicated by the linear approximation lines in Fig. 8. At lower temperature (350°C), a clear trend is not found. Larger resistivity changes for higher fields are not surprising and hardly conclusive for any interpretation. Rather, analysis of the two relaxation times may give further insight into the processes governing these changes. Figure 9 displays the temperature dependence of the decay time τ_1 for different voltages. For all voltages, a very similar temperature dependence is found and activation energies E_a ($\tau_1 \propto e^{E_a/kT}$) between 1.24 and 1.52 eV result (k =

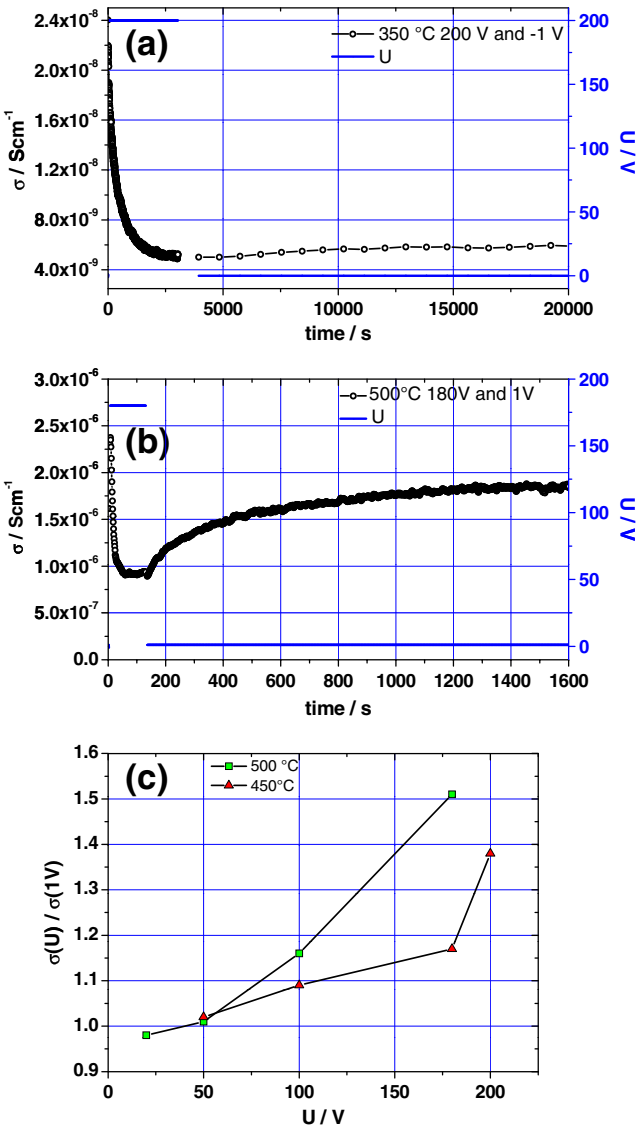

Fig. 6 (**a**) and (**b**) show the conductivity decrease under high voltages and conductivity relaxation under 1 V. (**a**) For 350°C, 200 V load, almost no relaxation is found. (**b**) At 500°C, relaxation takes place but is much slower than the conductivity decrease under 180 V. (**c**) Non-linearity of the conductivity for different temperatures; conductivity σ(U) reflects the situations right after applying the voltage U and is related to the 1 V value measured before high field stress (σ(1 V))

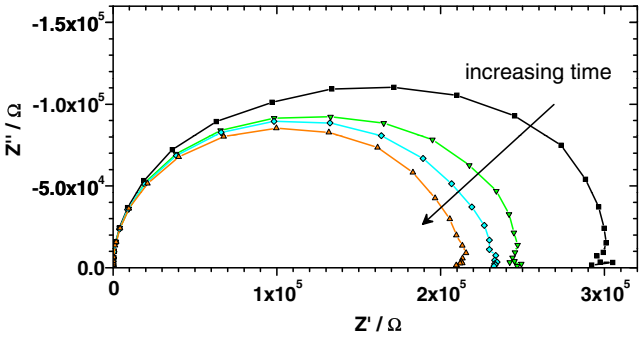

Fig. 7 Impedance spectra measured at 450°C after 152 s of high field stress (200 V). Significant distortion of the spectra due to the conductivity changes is observed and the relaxation is reflected by a shrinking size of the arcs. The spectra were measured 3, 9, 15, and 21 min after disconnecting the voltage

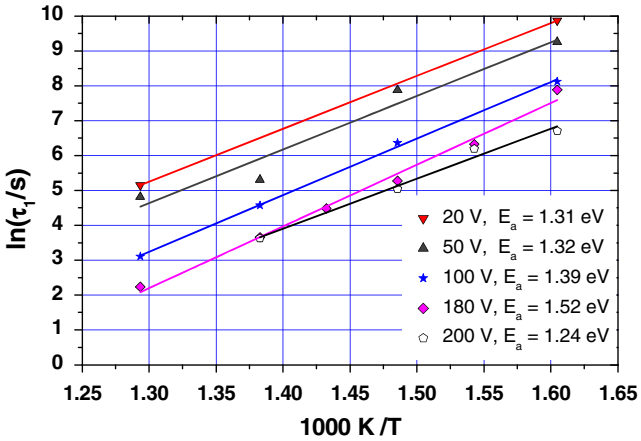

Fig. 9 Temperature dependence of the conductivity decay time τ_1 for different voltages. Linear regression lines and the corresponding activation energies are also given

Boltzmann's constant, T = temperature). It is also visible that τ_1 strongly depends on the voltage: For all temperatures, the conductivity decrease is much faster for larger fields. This field dependence is again visualized in Fig. 10. When quantifying the τ_1—U relation in terms of a power law

$$\tau_1 = \text{const} \cdot U^p \quad \Rightarrow \quad \log \tau_1 = \log(\text{const}) + p \cdot \log(U), \tag{3}$$

an exponent p of about −1.3 results for most temperatures.

The relaxation time τ_2 does not show a clear dependence on the voltage used during high field stress (Fig. 11(a)). However, it is again strongly temperature dependent (Fig. 11(b)) and an activation energy E'_a ($\tau_2 \propto e^{E'_a/kT}$) between 0.8 and 1.4 eV can be calculated. (Owing to the much slower relaxation and less accurate data, particularly at lower temperatures, the scatter is more pronounced than for the decay time τ_1.) The significant difference between the rate of conductivity decrease and conductivity relaxation, particularly for high voltages, is shown in Fig. 12 (τ_2 / τ_1 versus 1/T). For 180 Vand higher temperatures, the relaxation in nearly all cases required much more than ten times the decay time.

Changing the gas atmosphere from ambient air to 2.5% H_2 in Ar does not lead to qualitatively different conductivity variations under high field stress (Fig. 13(a)). However, the conductivity change becomes somewhat larger in hydrogen and also the decay time changes. For the test temperature of 450°C and 200 V, τ_1 increased in H_2/Ar by a factor of about 1.4. Repeated high voltage load also modified the conductivity change: it is shown in Fig. 13(b) that for successive high voltage load (60 s) and relaxation (1 h) experiments on one and the same PZT layer, the extent of the conductivity decrease becomes smaller. Moreover, the conductivity versus time curve changed when leaving the PZT sample at temperatures of about 450°C for several days. Figure 14(a) exemplarily demonstrates that during such a thermal equilibration the

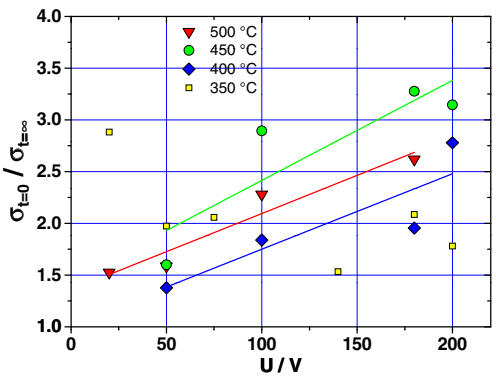

Fig. 8 Magnitude of the resistance increase (or conductivity decrease, respectively) for different voltages and temperatures

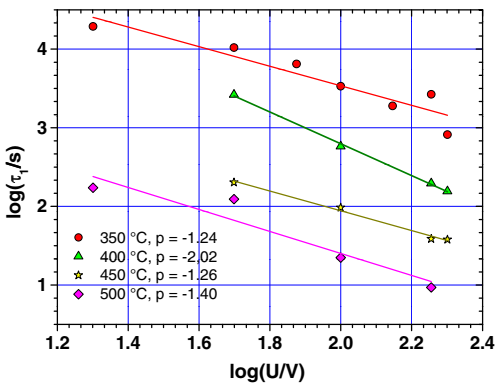

Fig. 10 Voltage dependence of the conductivity decay time τ_1 in a log-log plot for different temperatures. Lines reflect fits to Eq. 3 with exponent p

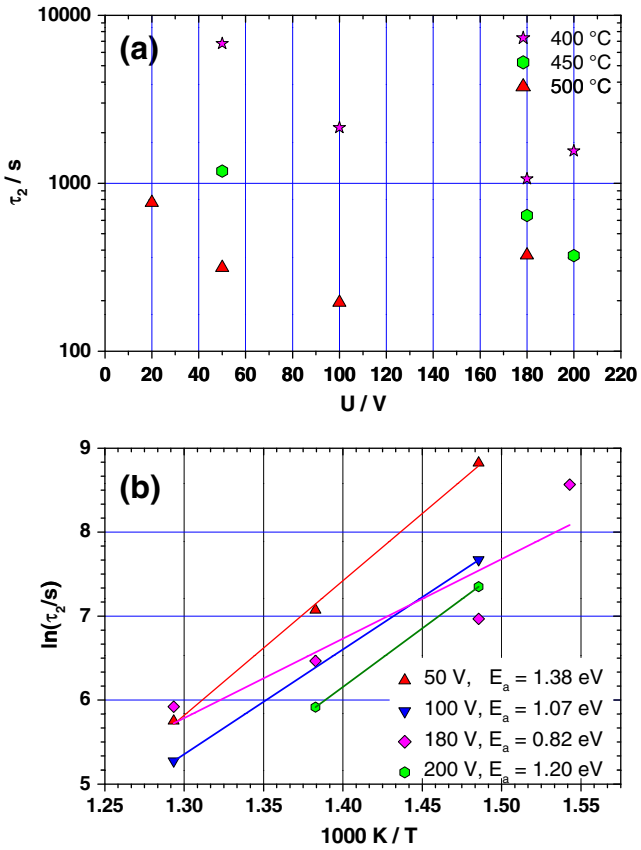

Fig. 11 (**a**) Voltage dependence of the relaxation time τ_2 for different temperatures. (**b**) Temperature dependence of the relaxation time τ_2 for different voltages. Linear regression lines and the corresponding activation energies are also given

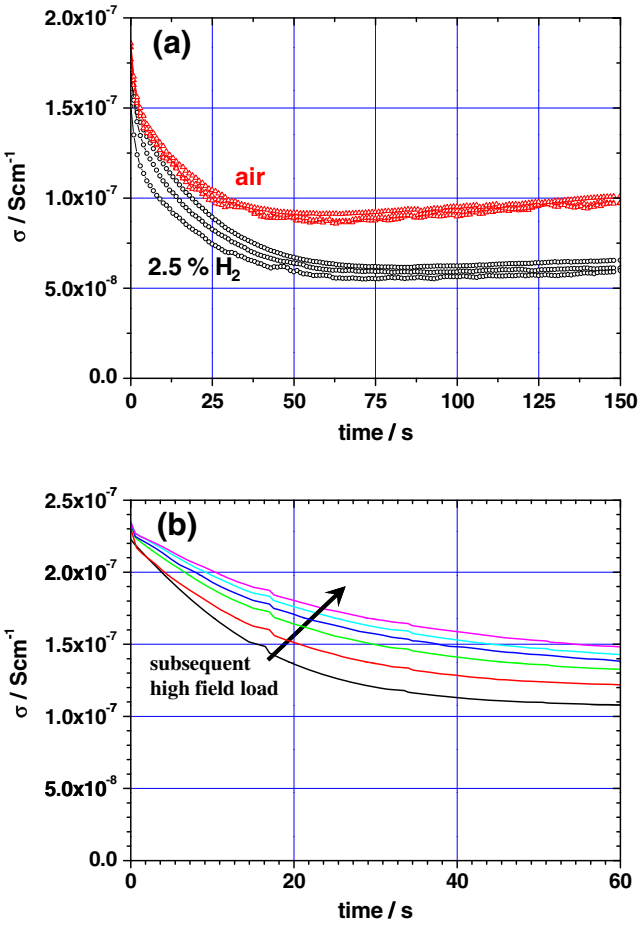

Fig. 13 (**a**) Conductivity decrease measured at 450°C and 200 V on different electrode pairs in air and in H_2 containing atmosphere. (**b**) Successive conductivity variation curves under 200 V load at 450°C, measured on one and the same PZT layer. Between each voltage load experiment, a 60 min relaxation took place at the same temperature

conductivity decrease become less pronounced. In addition, the small signal conductivity of a PZT layer without any high field load, measured by ac impedance spectroscopy, slowly decreased during annealing at 450°C (Fig. 14(b)). These additional measurements (Figs. 13 and 14) were performed on PZT pieces from a second batch of actuator stacks and with current flowing only in a single PZT layer (instead of two layers as sketched in Fig. 1(b)).

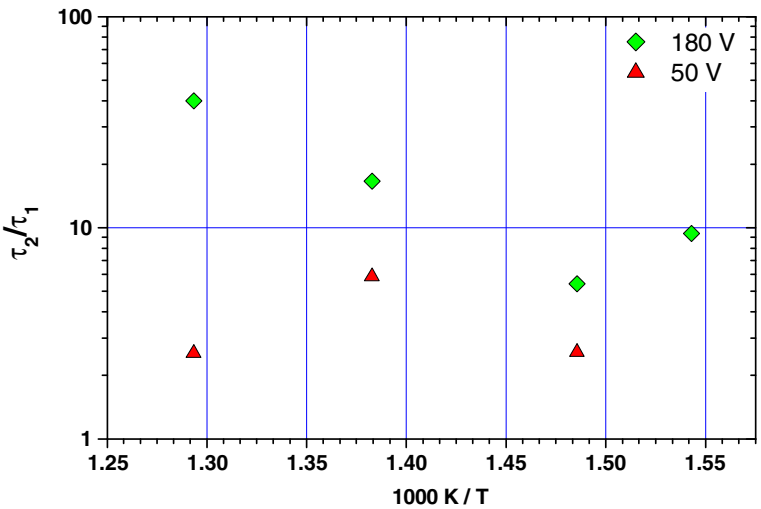

Fig. 12 Ratio between relaxation time τ_2 and decay time τ_1 for different temperatures and voltages, indicating that the relaxation is much slower, particularly for high voltages

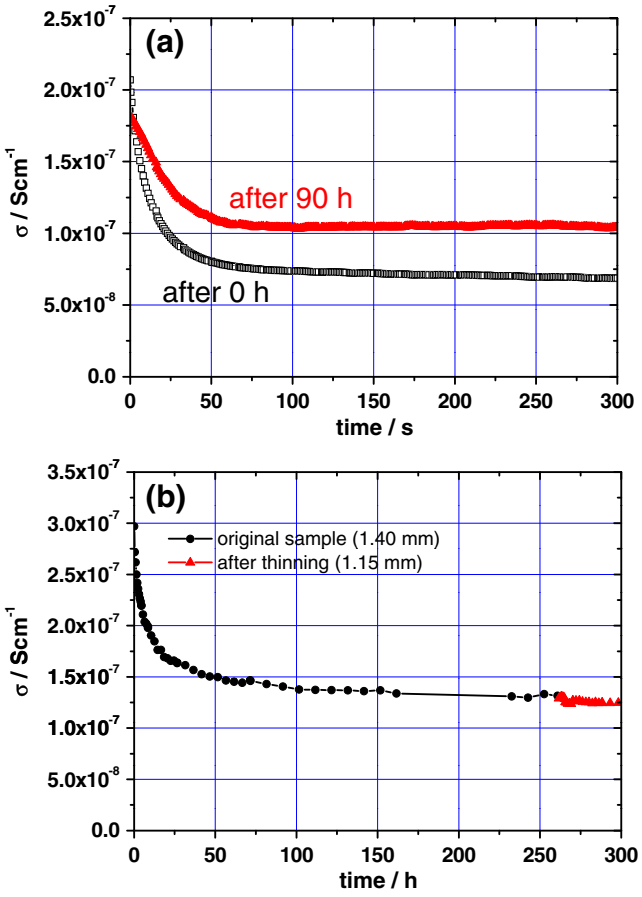

Fig. 14 (**a**) Change of the conductivity decrease due to 200 V load, measured on a PZT layer immediately after reaching the temperature of 450°C and on another layer after 90 h annealing at 450°C. (**b**) Variation of the small signal conductivity, measured by impedance spectroscopy, during annealing at 450°C in air

A last observation deals with the optical appearance of the PZT layers under high field load. A darkening was observable during conductivity decrease, and this darkened region again brightened during the relaxation process at temperatures above 400°C. When exposing

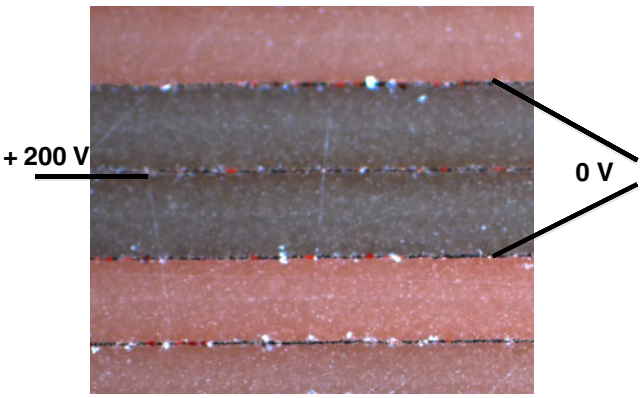

Fig. 15 Darkened pair of PZT layers after a conductivity decrease experiment under 200 V load at 450°C

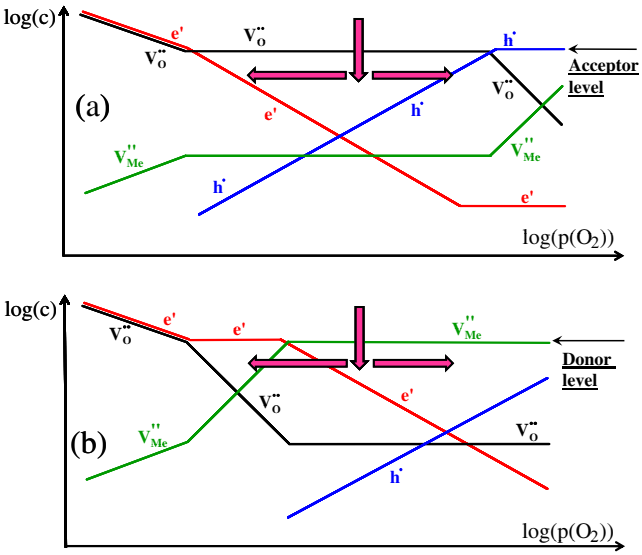

Fig. 16 Sketches of Brouwer diagrams of an acceptor-doped (**a**) and a donor-doped (**b**) metal oxide. The arrows indicate typical situations found for large band gap perovskites in air at high temperatures (*vertical arrows*), and symbolize changes due to stoichiometry polarization (*horiztonal arrows*)

the sample to temperatures of about 500°C, the darkening vanished more or less completely. Fig. 15 exemplarily shows a darkened area of a quenched sample after applying 200 V to the corresponding two PZT layers at 500°C. Spatial variations during darkening (e.g. a front moving between cathode and anode) could not be resolved but can also not be excluded. It can also not be excluded that the darkening is associated with the second degradation process on a much longer time scale which was mentioned above (Fig. 4(c)).

4 Discussion

As already discussed in the Introduction, the following two processes are candidates for time-dependent conductivity variations in oxides under high fields: i) Build-up of stoichiometry profiles and thus of spatially varying defect concentrations and ii) cation migration originating at electrodes, with formation of conducting paths or dendrites. Interestingly, the same two phenomena are also assumed to govern resistance changes in thin films of resistive switching devices [89–92]. For the temperatures used in this study (350–500°C), we consider water-based electrochemical dendrite formation as improbable. Moreover, in contradiction to our results, the averaged conductivity should increase during dendrite formation. Hence, we focus the following discussion to stoichiometry changes caused by defect motion. Such a stoichiometry polarization may either be carried by cation (lead) or anion (oxygen) vacancies. In $SrTiO_3$ and $BaTiO_3$, the A-site cation is comparatively

immobile due to high activation energies [13, 93–96]. While this does not necessarily allow a final conclusion regarding the Pb mobility in PZT, we nevertheless favor oxygen vacancies as the defect being able to cause internal concentration changes at the temperatures and on the time scales considered here.

Stoichiometry polarization in acceptor-doped $SrTiO_3$ and $BaTiO_3$ [48–51, 55, 56] can be understood from the schematic Brower diagram of an acceptor-doped metal oxide (Fig. 16(a)). Depending on the oxygen partial pressure, the acceptor is charge-compensated either by oxygen vacancies $V_O^{\bullet\bullet}$ or by holes $h^{\bullet}$. The vertical arrow in Fig. 16(a) indicates a typical defect chemical situation established in acceptor-doped $SrTiO_3$ at high temperatures in air [14]. Upon application of a voltage at lower temperatures using ionically blocking electrodes, such a material locally shifts into regimes of very low (cathode) and very high (anode) oxygen chemical potentials. This stoichiometry polarization is visualized in Fig. 16(a) by the horizontal arrows, even though one has to keep in mind that the field-induced internal stoichiometry changes take place at temperatures much lower than the equilibrium temperature for which the Brouwer diagram is sketched. For very low as well as for high chemical potentials, an enhanced conductivity can be found: in one case the electron (e') concentration is enhanced, in the other case the hole concentration [14, 50, 55]. Also with electrodes being only partial blocking for oxide ions, stoichiometry profiles can build-up [50, 56]. Accordingly, high field load can easily lead to a strong decrease of the overall resistance within a certain degradation time τ_1^*. After switching-off the field, re-equilibration of the acceptor-doped oxide takes place by chemical diffusion of oxygen on a longer time scale τ_2^*.

In donor-doped oxides (see typical Brouwer diagram in (Fig. 16(b)) [25, 26]), the situation is different. The donor is either charge compensated by metal vacancies, e.g. V''_{Me} (in PZT most probably lead vacancies of concentration $C_{V_{Pb}}$) or by electrons. The concentration of oxygen vacancies may be so small that their motion in a field does not significantly affect the other defect concentrations. Accordingly, absence of resistance degradation is observed in donor-doped $BaTiO_3$ and $SrTiO_3$ [48, 49, 57]. However, in PZT the pronounced PbO volatility according to

$$Pb_{Pb}^x + O_O^x \rightleftarrows PbO\uparrow + V''_{Pb} + V_O^{\bullet\bullet} \tag{4}$$

leads to a high value of the Schottky equilibrium constant

$$K_S = C_{V_{Pb}} \cdot C_{V_O} \tag{5}$$

and thus to a higher oxygen vacancy concentration C_{V_O} than in many other donor-doped perovskites [44, 97, 98]. Hence, the oxygen vacancy concentration may still be of relevance. Recent ^{18}O tracer experiments gave evidence of substantial oxygen diffusion and thus of a significant oxygen vacancy concentration level in similar donor-doped PZT stacks [47]. In donor-doped oxides, the (electronic) conductivity decreases with increasing partial pressure over a very broad chemical potential range (Fig. 16(b)). Stoichiometry polarization of PZT under high fields may thus enhance the (electronic) conductivity in one part of the sample and decrease it in the other (indicated by horizontal arrows in Fig. 16(b)). Effectively, this may either increase or decrease the total resistance, depending on specific conditions. PbO loss may even result in such a pronounced Schottky disorder of PZT (Eq. 5) that the material resembles a slightly acceptor-doped material with predominant hole conduction. The unknown K_S-value makes it difficult to predict, whether an effective conductivity increase or decrease has to be expected in donor-doped PZT under high fields.

Nevertheless, we can conclude that stoichiometry polarization of donor-doped PZT due to oxygen vacancy motion is a realistic scenario and may change the sample's resistance. Time τ_1 would then reflect the field-driven built-up of a stoichiometry profile and τ_2 the re-equilibration due to chemical diffusion. The following comparison of our results to data found for resistance degradation of acceptor-doped $SrTiO_3$ [48–50] shows that many quantitative similarities exist:

In acceptor-doped $SrTiO_3$, the degradation time τ_1^* is thermally activated with E_a being between 0.6 and 0.9 eV in single crystals [49] and ca. 1.2 eV in polycrystals [48]. Calculations suggest that the thermal activation of τ_1^* approximately reflects the activation energy of the oxygen vacancy mobility [50] (ca. 0.9 eV for slightly Fe-doped $SrTiO_3$ [1]). Activation energies of the τ_1 values found in this study are still within the same range (1.2–1.5 eV).

In single crystalline Ni-doped $SrTiO_3$, an exponent of −1.1 is found for the power law relation between degradation time τ_1^* and electric field at 180°C [49], cf. Eq. 3. According to numerical modeling, a linear inverse relation between τ_1^* and field is expected [50]. In polycrystalline acceptor-doped $SrTiO_3$, exponents are much larger (−2.45) [48], which was attributed to the strongly blocking character of grain boundaries in this material: space charge layers with depletion of positive charge carriers hinder oxide ions to pass the boundaries. In our polycrystalline PZT, an exponent p of approximately −1.3 is found which is close to that of single crystalline $SrTiO_3$. This may indicate that the space charges at grain boundaries of our PZT are not blocking for oxygen vacancies, in accordance with the fact that donor-doped material often exhibits a depletion of negative charge carriers in space charges [99–102]. Rather, fast ion transport along grain boundaries with oxygen vacancy accumulation in space charge zones may

be expected. Fast oxygen tracer diffusion along grain boundaries was indeed found in similar PZT stacks at higher temperatures [47].

In acceptor-doped $SrTiO_3$, conductivity relaxation is caused by chemical (ambipolar) diffusion of oxygen back to a homogeneous oxygen stoichiometry [55] and is much slower than the field-driven built-up of the modified conductivity. The relaxation time τ_2^* is thermally activated in accordance with the chemical diffusion coefficient. In our study, the relaxation is also much slower than the conductivity decrease and the activation energy of τ_2 is of the order of 1.1 eV. This is close to the value of about 1.2 eV, which can be evaluated from chemical diffusion data of a similarly doped PZT material [45].

For further analysis, we calculate diffusion coefficients from the two measured time constants τ_1 and τ_2: For a given diffusion length $L_D \approx \sqrt{2\widetilde{D}t}$ and relaxation time t = τ_2, we can roughly estimate a diffusion constant $\widetilde{D}$ from

$$\widetilde{D} \approx \frac{{L_D}^2}{2\tau_2}. \tag{6}$$

According to our interpretation in terms of stoichiometry polarization, $\widetilde{D}$ should correspond to the chemical diffusion coefficient of oxygen and the diffusion length can then be approximated by the layer thickness. For 450°C set temperature (i.e. $\tau_2 \approx 700$ s), we get a chemical diffusion coefficient of ca. $4 \cdot 10^{-8}$ cm^2/s. This value is in agreement with the diffusion coefficient estimated from the equilibration experiment shown in (Fig. 14(b)): The thermodynamic equilibrium state at 450°C in air has to differ from the defect chemical situation established during preparation under reducing conditions at much higher temperatures. Hence, the conductivity decrease with a decay time of about 10 h can be interpreted as defect chemical equilibration of the oxygen stoichiometry. Removal of about 18% of the material after equilibration lead to the same conductivity values (cf. Fig. 14(b)) and thus we conclude that indeed the whole bulk of the sample was involved in this conductivity change. From Eq. 6, with π^2 instead of the factor 2 [20] and L_D as sample thickness, we may again estimate the chemical diffusion coefficient and get a value of about $5 \cdot 10^{-8}$ cm^2/s. These values are also within the extrapolated range of chemical diffusion coefficients reported in Ref. [45] for a similarly doped though differently prepared PZT (about 10^{-6} cm^2/s).

A modeling study on stoichiometry polarization in acceptor-doped $SrTiO_3$ [50] showed that, to a first approximation, the velocity (v) of a concentration front moving in high fields (E) is related to the mobility of oxygen vacancies (u_V) via $u_V = v/E$. Assuming that τ_1 approximates the time a concentration front needs to move through the sample of thickness L, the velocity is given by L/τ_1, and using Nernst-Einstein's equation we expect the oxygen vacancy diffusion coefficient

$$D_V = \frac{kT}{2e} u_V = \frac{kTL}{2e\tau_1 E}. \tag{7}$$

Symbol e denotes the elementary charge. For 450°C set temperature, we can calculate a vacancy diffusion coefficient of ca. $2 \cdot 10^{-10}$ cm^2/s from Eq. 7, which is more than two orders of magnitude lower than the chemical diffusion coefficient estimated above. This might still be realistic, since chemical diffusion coefficients can significantly exceed the vacancy diffusion coefficients [103]. However, the value is also much smaller than the vacancy diffusion coefficient of slightly Fe-doped $SrTiO_3$ (about $4 \cdot 10^{-7}$ cm^2/s at such a temperature) [1]. Hence, also other possible reasons for the rather small value of D_V may be worth considering. For example, in case of fast oxygen transport in or along grain boundaries of PZT, Eq. 7 might not be appropriate for calculating D_V.

Also the effects of hydrogen, successive high voltage load and thermal equilibration on the conductivity versus time curves (Figs. 13 and 14) can be explained by the model of stoichiometry polarization: Strongly ion-blocking electrodes are certainly realistic in a stack with many PZT layers and Cu inner electrodes, but complete oxygen blocking is not expected; at least close to the three phase boundaries, i.e. at the surface or in any pores of the Cu electrodes, some oxygen incorporation or release should take place. Therefore, an influence of the gas atmosphere on the conductivity variation upon field load can be expected; hydrogen leads to a complete blocking of the cathodic oxygen reduction reaction and may thus intensify conductivity changes (Fig. 13(a)). Moreover, the rates of residual cathodic and anodic reactions of oxide ions can easily be non-symmetric also in air, and hence the total amount of oxygen vacancies in the material may vary during a polarization experiment. Accordingly, a subsequent polarization (after relaxation) can be expected to lead to a different curve: For more cathodic oxygen incorporation than anodic oxygen release, the total amount of oxygen vacancies would decrease during each polarization step and may cause less conductivity change in the next experiment, in agreement with Fig. 13(b). Also thermal equilibration modifies the oxygen vacancy content and a decrease of the vacancy concentration with time can be expected in air for a material prepared under reducing conditions. Accordingly, the conductivity variation should become less pronounced with annealing time. This is again in agreement with measurement results (Fig. 14(a)). In summary, qualitative as well as quantitative analysis shows satisfying agreement with our hypothesis that the phenomena described in this paper are associated with field-driven stoichiometry polarization, i.e. oxygen vacancy accumulation

near cathodes and/or depletion near anodes and with diffusive relaxation after switching-off the voltage.

5 Conclusions

The conductivity of donor-doped PZT stacks with Cu inner electrodes decreased under high fields and the corresponding time constants show a characteristic dependence on temperature and voltage: The higher the voltage, the faster the Arrhenius-activated conductivity decrease. Also the surrounding gas atmosphere and pre-annealing affected the conductivity changes. After disconnecting the high voltage, the conductivity again relaxes on a longer time scale. The similarities between voltage, time and temperature dependences found here and high field conductivity changes in accepter-doped $SrTiO_3$ suggest that in both cases motion of oxygen vacancies and thus stoichiometry variations play the major role. Quantitative estimates of oxygen diffusion coefficients are reasonable and also effects of successive polarization and pre-annealing could be explained. While the suggested importance of oxygen vacancies might be unexpected for donor-doped material, it is nevertheless believed to be realistic, since the high PbO volatility of PZT can easily lead to a significant oxygen vacancy concentration, despite donor doping. It is an open question whether this suggested vacancy motion mainly occurs in/near grain boundaries or in the grain interior. Key to this study was the ability to make systematic measurements by accessing and applying high fields to multiple individual electrode pairs within a given PZT stack.

Acknowledgements The authors gratefully acknowledge funding by the Christian Doppler Research Association.

References

1. I. Denk, W. Muench, J. Maier, J. Am. Ceram. Soc. **78**, 3265 (1995)
2. R. Merkle, J. Maier, Phys. Chem. Chem. Phys. **5**, 2297 (2003)
3. R.A. De Souza, J. Fleig, R. Merkle, J. Maier, Zeitschrift fuer Metallkunde/Materials Research and Advanced Techniques **94**, 218 (2003)
4. R.A. De Souza, J. Fleig, J. Maier, O. Kienzle, Z. Zhang, W. Sigle, M. Ruhle, J. Am. Ceram. Soc. **86**, 922 (2003)
5. M. Vollmann, R. Hagenbeck, R. Waser, J. Am. Ceram. Soc. **80**, 2301 (1997)
6. R. Waser, J. Am. Ceram. Soc. **74**, 1934 (1991)
7. R. Meyer, R. Waser, J. Helmbold, G. Borchardt, J. Electroceram. **9**, 101 (2002)
8. J. Daniels, R. Wernicke, Philips Res. Rep. **31**, 544 (1976)
9. S. Rodewald, J. Fleig, J. Maier, J. Am. Ceram. Soc. **84**, 521 (2001)
10. H.S. Kwon, H.I. Yoo, C.H. Kim, K.H. Hur, J. Appl. Phys. **107**, 083702 (2010)
11. C.J. Shin, H.I. Yoo, C.E. Lee, Solid State Ionics **178**, 1081 (2007)
12. H.I. Yoo, C.E. Lee, J. Am. Ceram. Soc. **88**, 617 (2005)
13. R. Moos, K.H. Haerdtl, J. Am. Ceram. Soc. **80**, 2549 (1997)
14. G.M. Choi, H.L. Tuller, J. Am. Ceram. Soc. **71**, 201 (1988)
15. J. Maier, J. Jamnik, M. Leonhardt, Solid State Ionics **129**, 25 (2000)
16. K. Sasaki, J. Maier, J. Europ. Ceram. Soc. **19**, 741 (1999)
17. K.D. Becker, M. Schrader, H.S. Kwon, H.I. Yoo, Phys. Chem. Chem. Phys. **11**, 3082 (2009)
18. G.Y. Yang, E.C. Dickey, C.A. Randall, D.E. Barber, P. Pinceloup, M.A. Henderson, R.A. Hill, J.J. Beeson, D.J. Skamser, J. Appl. Phys. **96**, 7492 (2004)
19. I.J. Clark, F.B. Marques, D.C. Sinclair, J. Europ. Ceram. Soc. **22**, 579 (2002)
20. W. Preis, W. Sitte, Solid State Ionics **177**, 3093 (2006)
21. Y. Tsur, C.A. Randall, J. Am. Ceram. Soc. **84**, 2147 (2001)
22. F.D. Morrison, A.M. Coats, D.C. Sinclair, A.R. West, J. Electroceram. **6**, 219 (2001)
23. Y.M. Chiang, T. Takagi, J. Am. Ceram. Soc. **73**, 3278 (1990)
24. Y. Tsur, T.D. Dunbar, C.A. Randall, J. Electroceram. **7**, 25 (2001)
25. D.M. Smyth, J. Electroceram. **9**, 179 (2002)
26. J. Daniels, K.H. Haerdtl, Philips Res. Repts. **31**, 489 (1976)
27. B.A. Boukamp, M.T.N. Pham, D.H.A. Blank, H.J.M. Bouwmeester, Solid State Ionics **170**, 239 (2004)
28. M.V. Raymond, D.M. Smyth, J. Phys. Chem. Solids **57**, 1507 (1996)
29. M.V. Raymond, D.M. Smyth, Integrated Ferroelectrics **4**, 145 (1994)
30. R.V. Wang, P.C. McIntyre, J. Appl. Phys. **97**, 023508 (2005)
31. T. Izaki, H. Haneda, A. Watanabe, J. Tanaka, S. Shirasaki, K. Tsuji, Nippon Seramikkusu Kyokai Gakujutsu Ronbunshi-Journal of the Ceramic Society of Japan **101**, 133 (1993)
32. R.L. Holman, R.M. Fulrath, J. Appl. Phys. **44**, 5227 (1973)
33. S. Zhao, S.J. Zhang, W. Liu, N.J. Donnelly, Z. Xu, C.A. Randall, J. Appl. Phys. **105**, 053705 (2009)
34. M.F. Zhang, Y. Wang, K.F. Wang, J.S. Zhu, J.M. Liu, J. Appl. Phys. **105**, 061639 (2009)
35. V.V. Prisedsky, V.I. Shishkovsky, V.V. Klimov, Ferroelectrics **17**, 465 (1978)
36. B. Guiffard, E. Boucher, L. Eyraud, L. Lebrun, D. Guyomar, J. Europ. Ceram. Soc. **25**, 2487 (2005)
37. D. Kobor, B. Guiffard, L. Lebrun, A. Hajjaji, D. Guyomar, J. Phys. D-Appl. Phys. **40**, 2920 (2007)
38. R.A. Roca, E.R. Botero, F. Guerrero, J.D.S. Guerra, D. Garcia, J. A. Eiras, J. Phys. D-Appl. Phys. **41**, 045410 (2008)
39. J.J. Dih, R.M. Fulrath, J. Am. Ceram. Soc. **61**, 448 (1978)
40. J.G. Burt, R.A. Krakowsky, J. Am. Ceram. Soc. **54**, 415 (1971)
41. A.P. Barranco, F.C. Pinar, O.P. Martinez, J.D.S. Guerra, I.G. Carmenate, J. Europ. Ceram. Soc. **19**, 2677 (1999)
42. R.W. Whatmore, O. Molter, C.P. Shaw, J. Europ. Ceram. Soc. **23**, 721 (2003)
43. A. Ezis, J.G. Burt, R.A. Krakowsky, J. Am. Ceram. Soc. **53**, 521 (1970)
44. N.J. Donnelly, C.A. Randall, J. Appl. Phys. **109** (2011)
45. N.J. Donnelly, C.A. Randall, Appl. Phys. Lett. **96** (2010)
46. S. Gottschalk, H. Hahn, S. Flege, A.G. Balogh, J. Appl. Phys. **104**, 114106 (2008)
47. T. Froemling, A. Schintlmeister, H. Hutter, J. Fleig, J. Am. Ceram. Soc. **94**, 1173 (2011)
48. R. Waser, T. Baiatu, K.-H. Haerdtl, J. Am. Ceram. Soc. **73**, 1645 (1990)
49. R. Waser, T. Baiatu, K.-H. Haerdtl, J. Am. Ceram. Soc. **73**, 1654 (1990)
50. T. Baiatu, R. Waser, K.-H. Haerdtl, J. Am. Ceram. Soc. **73**, 1663 (1990)
51. J. Rodel, G. Tomandl, J. Mat. Sci. **19**, 3515 (1984)
52. M.H. Hebb, J Chem Phys **20**, 185 (1952)

53. C. Wagner, Proc. 7th Meeting of Int. Conf. on Electrochemical Thermodynamics and Kinetics, Lindau, 1955, Butterworth, London, 361 (1956)
54. I. Yokota, J. Phys. Soc. Jpn. **16**, 2213 (1961)
55. S. Rodewald, J. Fleig, J. Maier, J. Am. Ceram. Soc. **83**, 1969 (2000)
56. S. Rodewald, N. Sakai, K. Yamaji, H. Yokokawa, J. Fleig, J. Maier, J. Electroceram. **7**, 95 (2001)
57. J.B. MacChesney, P.K. Gallagher, F.V. Dimarcello, J. Am. Ceram. Soc. **46**, 197 (1963)
58. D.Y. Zheng, J. Swingler, P. Weaver, Sensor Actuat A-Phys **158**, 106 (2010)
59. N.J. Donnelly, C.A. Randall, J. Am. Ceram. Soc. **92**, 405 (2009)
60. I.P. Lipscomb, P.M. Weaver, J. Swingler, J.W. McBride, Sensor Actuat A-Phys **151**, 179 (2009)
61. J. Thongrueng, T. Tsuchiya, K. Nagata, Jpn. J. Appl. Phys. Part 1 - Regul. Pap. Short Notes Rev. Pap. 37, 5306 (1998)
62. J. Pritchard, C.R. Bowen, F. Lowrie, Br. Ceram. Trans. **100**, 265 (2001)
63. I.P. Lipscomb, P.M. Weaver, J. Swingler, J.W. McBride, J. Electroceram. **23**, 72 (2009)
64. H.C. Ling, A.M. Jackson, IEEE Trans Compon Hybrids Manuf Technol **12**, 130 (1989)
65. H. Kanai, O. Furukawa, S. Nakamura, Y. Yamashita, J. Am. Ceram. Soc. **76**, 459 (1993)
66. J.L. Cao, L.T. Li, N.X. Zhang, Z.L. Gui, J. Mater. Res. **17**, 779 (2002)
67. H. Kanai, O. Furukawa, S. Nakamura, M. Hayashi, M. Yoshiki, Y. Yamashita, J. Am. Ceram. Soc. **78**, 1173 (1995)
68. S. Yang, J. Wu, A. Christou, Microelectron. Reliab. **46**, 1915 (2006)
69. S.J. Krumbein, IEEE Trans Compon Hybrids Manuf Technol **11**, 5 (1988)
70. J.C. Lin, J.Y. Chan, Mater. Chem. Phys. **43**, 256 (1996)
71. S.A. Yang, A. Christou, IEEE Trans. Device Mater. Reliab. **7**, 188 (2007)
72. G.T. Kohman, H.W. Hermance, G.H. Downes, Bell Syst Tech J **34**, 1115 (1955)
73. C. Dominkovics, G. Harsanyi, Microelectron. Reliab. **48**, 1628 (2008)
74. G. Harsanyi, IEEE Trans Compon. Packag. Manuf. Technol. Part A **18**, 602 (1995)
75. R.C. Benson, B.M. Romenesko, J.A. Weiner, B.H. Nall, H.K. Charles, IEEE Trans Compon Hybrids Manuf Technol **11**, 363 (1988)
76. M.T. Chentir, E. Bouyssou, L. Ventura, C. Anceau, J. Appl. Phys. **105**, 061605 (2009)
77. P. Zubko, D.J. Jung, J.F. Scott, J. Appl. Phys. **100**, 114113 (2006)
78. B. Nagaraj, S. Aggarwal, T.K. Song, T. Sawhney, R. Ramesh, Phys. Rev. B **59**, 16022 (1999)
79. F.S. Baumann, J. Fleig, H.U. Habermeier, J. Maier, Solid State Ionics **177**, 1071 (2006)
80. J. Fleig, F.S. Baumann, V. Brichzin, H.R. Kim, J. Jamnik, G. Cristiani, H.U. Habermeier, J. Maier, Fuel Cells **6**, 284 (2006)
81. A.K. Opitz, J. Fleig, Solid State Ionics **181**, 684 (2010)
82. J. Maier, Berichte der Bunsengesellschaft/Phys Chem. Chem Phys **90**, 26 (1986)
83. J. Fleig, J. Maier, Phys. Chem. Chem. Phys. **1**, 3315 (1999)
84. J. Fleig, Solid State Ionics **161**, 279 (2003)
85. P. Balaya, J. Jamnik, J. Fleig, J. Maier, J. Electrochem. Soc. **154**, P69 (2007)
86. P. Balaya, J. Jamnik, J. Fleig, J. Maier, Appl. Phys. Lett. **88**, 062109 (2006)
87. J.-S. Lee, J. Fleig, J. Maier, D.-Y. Kim, T.-J. Chung, J. Am. Ceram. Soc. **88**, 3067 (2005)
88. J.-S. Lee, J. Fleig, J. Maier, T.-J. Chung, D.-Y. Kim, Solid State Ionics **176**, 1711 (2005)
89. R. Waser, R. Dittmann, G. Staikov, K. Szot, Adv. Mater. **21**, 2632 (2009)
90. C. Schindler, X. Guo, A. Besmehn, R. Waser, Z. Phys. Chemie-Int. J. Res. Phys. Chem. Chem. Phys. **221**, 1469 (2007)
91. R. Waser, M. Aono, Nat. Mater. **6**, 833 (2007)
92. K. Szot, W. Speier, G. Bihlmayer, R. Waser, Nat. Mater. **5**, 312 (2006)
93. R. Wernicke, Phys. Status Solidi A-Appl. Res. **47**, 139 (1978)
94. R. Wernicke, Philips Res Rep **31**, 526 (1976)
95. K. Gomann, G. Bochardt, M. Schulz, A. Gomann, W. Maus-Friedrichs, B. Lesage, O. Kaitasov, S. Hoffman-Eifert, T. Schneller, Phys. Chem. Chem. Phys. **7**, 2053 (2005)
96. S. Koerfer, R.A. De Souza, H.I. Yoo, M. Martin, Solid State Sci. **10**, 725 (2008)
97. K.H. Hardtl, H. Rau, Solid State Commun. **7**, 41 (1969)
98. D.A. Northrop, J. Am. Ceram. Soc. **50**, 441 (1967)
99. W. Preis, W. Sitte, Solid State Ionics **177**, 2549 (2006)
100. Y.M. Chiang, T. Takagi, J. Am. Ceram. Soc. **73**, 3286 (1990)
101. W. Heywang, J. Am. Ceram. Soc. **47**, 484 (1964)
102. G.V. Lewis, C.R.A. Catlow, R.E.W. Casselton, J. Am. Ceram. Soc. **68**, 555 (1985)
103. J. Maier, Physical Chemistry of Ionic Materials - Ions and Electrons in Solids, John Wiley & Sons, Ltd (2005)